Supporting information

Large area arrays of discrete single-molecule junctions derived from host-guest complexes

Enrique Escorihuela,[1,2] Jesús del Barrio[1,3], Ross J. Davidson,[4] Andrew Beeby,[4] Paul J. Low,[5] Francesc Prez-Murano,[6] Pilar Cea,[1,2,7,*] Santiago Martin.[1,2,7,*]

[1] *Instituto de Nanociencia y Materiales de Aragón (INMA), CSIC-Universidad de Zaragoza, 50009, Zaragoza, Spain.*
[2] *Departamento de Química Física, Universidad de Zaragoza, 50009, Zaragoza, Spain.*
[3] *Departamento de Química Orgánica, Universidad de Zaragoza, 50009, Zaragoza, Spain.*
[4] *Department of Chemistry, Durham University, South Rd, Durham, DH1 3LE, UK.*
[5] *School of Molecular Sciences, University of Western Australia, 35 Stirling Highway, Crawley, 6009, Western Australia, Australia.*
[6] *Institute of Microelectronics of Barcelona (IMB-CNM, CSIC), 08193, Bellaterra, Spain.*
[7] *Laboratorio de Microscopias Avanzadas (LMA), Universidad de Zaragoza, 50018, Zaragoza, Spain.*

S1. Characterization of 1[Cl]$_2$−CB[7] interaction in solution

Fluorescence Spectroscopy

The fluorescent emission of **[1]**[Cl]$_2$ in aqueous solutions demonstrates an enhancement upon the addition of **CB[7];** similar observations have been made concerning p-tolyl-viologen derivatives upon host-guest inclusion.[1-2]

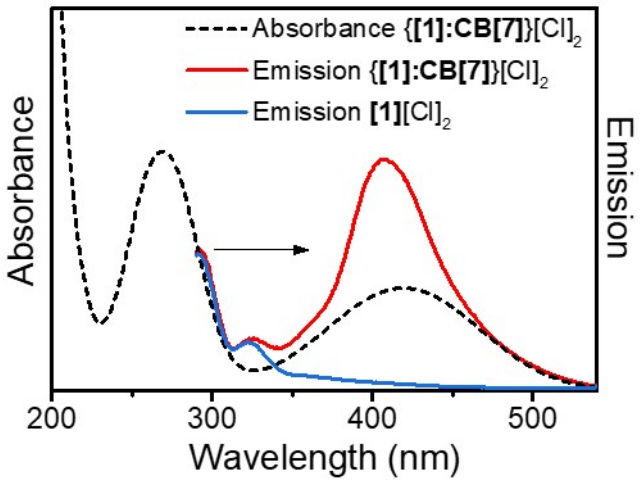

Figure S1. Emission spectra of **[1]**[Cl]$_2$ and {**[1]:CB[7]**}[Cl]$_2$ in 10^{-6} M aqueous solution and absorbance spectrum of {**[1]:CB[7]**}[Cl]$_2$.

The supramolecular assembly of **CB[7]** and **[1]**[Cl]$_2$ was monitored by ITC (Figure S2). The upper plot shows the thermogram (thermal power as a function of time) and the lower panel shows the binding isotherm, *i.e.* **CB[7]**-normalized heat effect per injection as a

function of molar ratio. The equilibrium constants and enthalpies were obtained from the fitting to a cooperative binding model (Table S1).[3] Experiments were carried out in water at 25 °C.

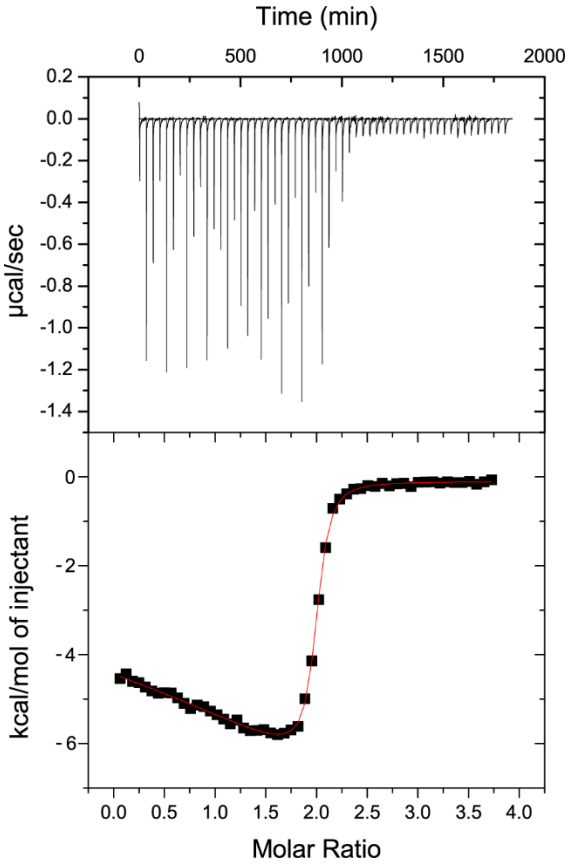

Figure S2. Calorimetric titration for the {**[1]:CB[7]**}$[Cl]_2$ interaction. The titration was carried out in water at 25 °C.

Table 1. Thermodynamic parameters for the interaction between **CB[7]** and **[1]**$[Cl]_2$ as determined by ITC.

Host–Guest Interaction	K_a (10^7) (M^{-1})	α	ΔH (kcal/mol)	Δh (kcal/mol)
1^{2+} + 2CB[7] → $CB[7]_2$:1^{2+}	1.2	0.72	-1.05	-0.4

The titrations were carried out in water at 25 °C. K_a and α are the site-specific association constant and the cooperativity constant respectively. The site-specific binding enthalpy and cooperativity enthalpy are ΔH and Δh respectively. Relative error in the site-specific association constant is 10%.

S2. QCM measurements to determine the surface coverage of a {[1]:CB[7]}[Cl]$_2$ SAM.

To evaluate and follow the formation of a SAM of {**[1]:CB[7]**}[Cl]$_2$, a gold quartz crystal microbalance (QCM) substrate was incubated in a 10^{-6} M solution of {**[1]:CB[7]**}[Cl]$_2$ and the variation in the resonator frequency was monitored with the time (Figure S3). The response of the QCM frequency to a change in mass of the resonator is given by Sauerbrey equation[4] (Eq. 1)

$$\Delta f = -\frac{2 \cdot f_0^2 \cdot \Delta m}{A \cdot \rho_q^{1/2} \cdot \mu_q^{1/2}} \qquad \text{(Eq. 1)}$$

where f_0 is the fundamental resonant frequency of ca. 5 MHz, Δm(g) is the change in mass, A is the area of the electrode, μ_q is the shear modulus (2.95×10^{11} dyn/cm^2), ρ_q is the density of the quartz (2.65 g/cm^3), and the molecular weights of **1** and **CB[7]** are 473.5 and 1162.96 g/mol, respectively.

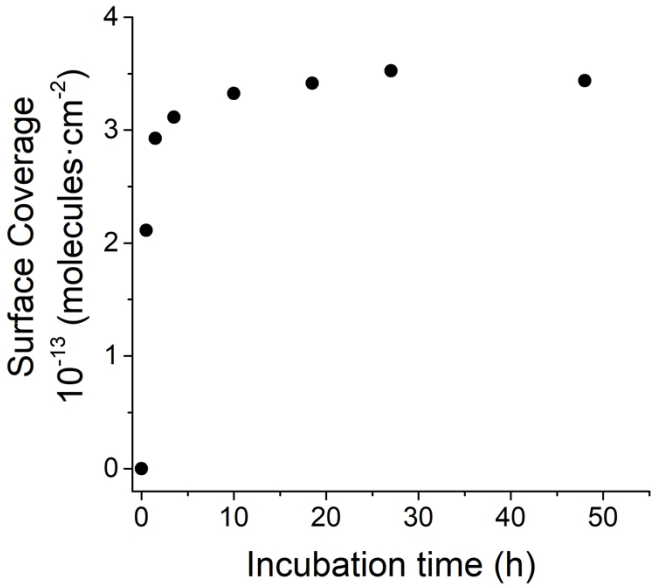

Figure S3. Surface coverage vs. time for a QCM resonator incubated in a 10^{-6} M solution of {**[1]:CB[7]**}[Cl]$_2$

S3. {[1]:CB[7]}$[Cl]_2$ surface coverage

A bearing analysis of the AFM images was made in order to calculate the {**[1]:CB[7]**}$[Cl]_2$ surface coverage (Figure S4). In a bearing analysis, the depths of all pixels of the image with respect to a reference point, i.e., the highest pixel, are analysed to give an accurate estimation of the percentage of area covered by features, i.e. surface coverage, at every pixel depth. From the images in Figure S4 a surface coverage of 95 ± 1 % is determined

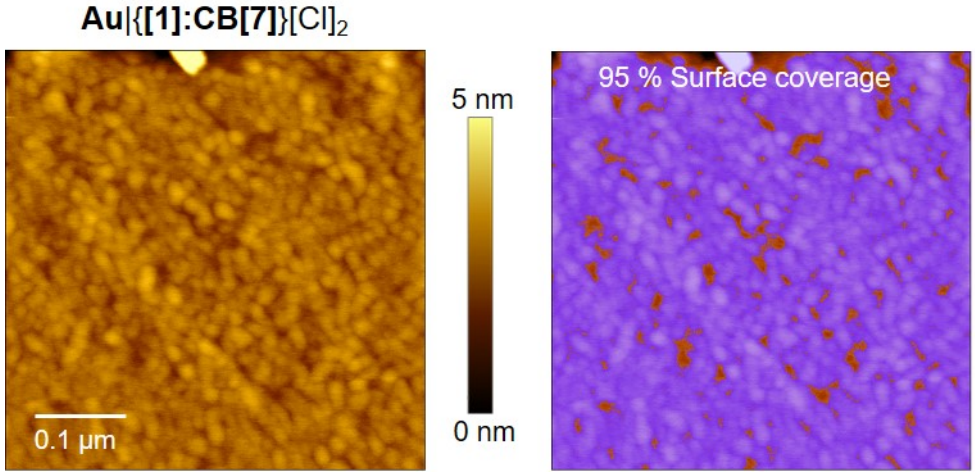

Figure S4. A 500x500 nm^2 AFM image of a {**[1]:CB[7]**}$[Cl]_2$ film without (left) and with the mask in blue revealing film-free areas (right).

S4. Thickness of a {[1]:CB[7]}$[Cl]_2$ SAM.

The thickness of {[1]:CB[7]}[Cl]2 SAM on the gold substrates was estimated using the attenuation of the Au4*f* signal according to: $I_{SAM} = I_{substrate} \exp(-d/\lambda \sin \theta)$, where d is the film thickness, I_{SAM} and $I_{substrate}$ are the average of the intensities of the Au4*f* 5/2 and Au4*f* 7/2 peaks attenuated by the SAM and from clean gold, respectively, θ is the photoelectron take-off angle, and λ = 4.2 ± 0.1 nm,[5] is the effective attenuation length of the photoelectron (Figure S4). A thickness value of (1.50 ± 0.04) nm was obtained, in agreement with the formation of a monolayer of {**[1]:CB[7]**}$[Cl]_2$ as the molecular length of **1** is 1.95 nm as determined by Spartan´08.

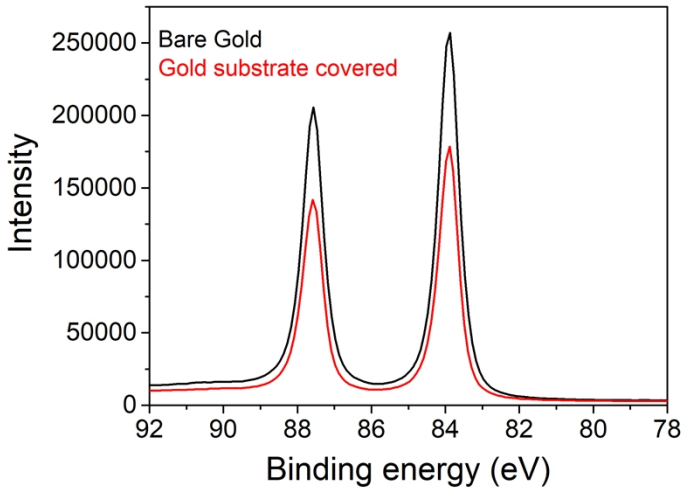

S5. Incorporation of gold nanoparticles (AuNPs)

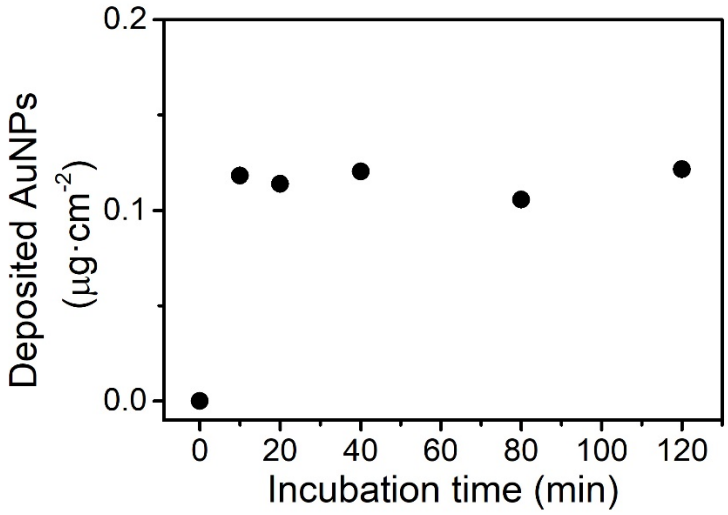

Figure S6. Surface density of gold nanoparticles as deposited onto a {**[1]:CB[7]**}$[Cl]_2$ film immersed in a dispersion of AuNPs vs. the incubation time.

Diameter and height of the AuNPs

Diameters and heights of AuNPs were obtained by using height profiles across an AFM image as shown in Figure 2b over more than 200 individual particles. The statistical analysis of the data extracted from AFM image allows us to conclude that these AuNPs exhibit an average diameter of 5.5 ± 2 nm (corrected by the tip convolution[6]) and an average height of 4.1 ± 2 nm. Histograms showing the diameter and height value distributions are depicted in Figure S7.

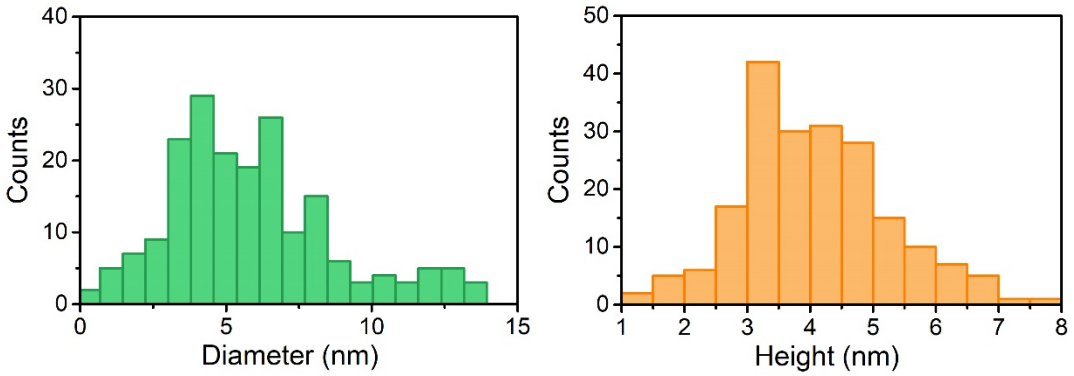

Figure S7. Histograms showing the particle diameter (corrected by the tip convolution), and height distributions, corresponding to over more than 200 individual particles.

Incorporation of AuNPs onto a [1][Cl]$_2$ film

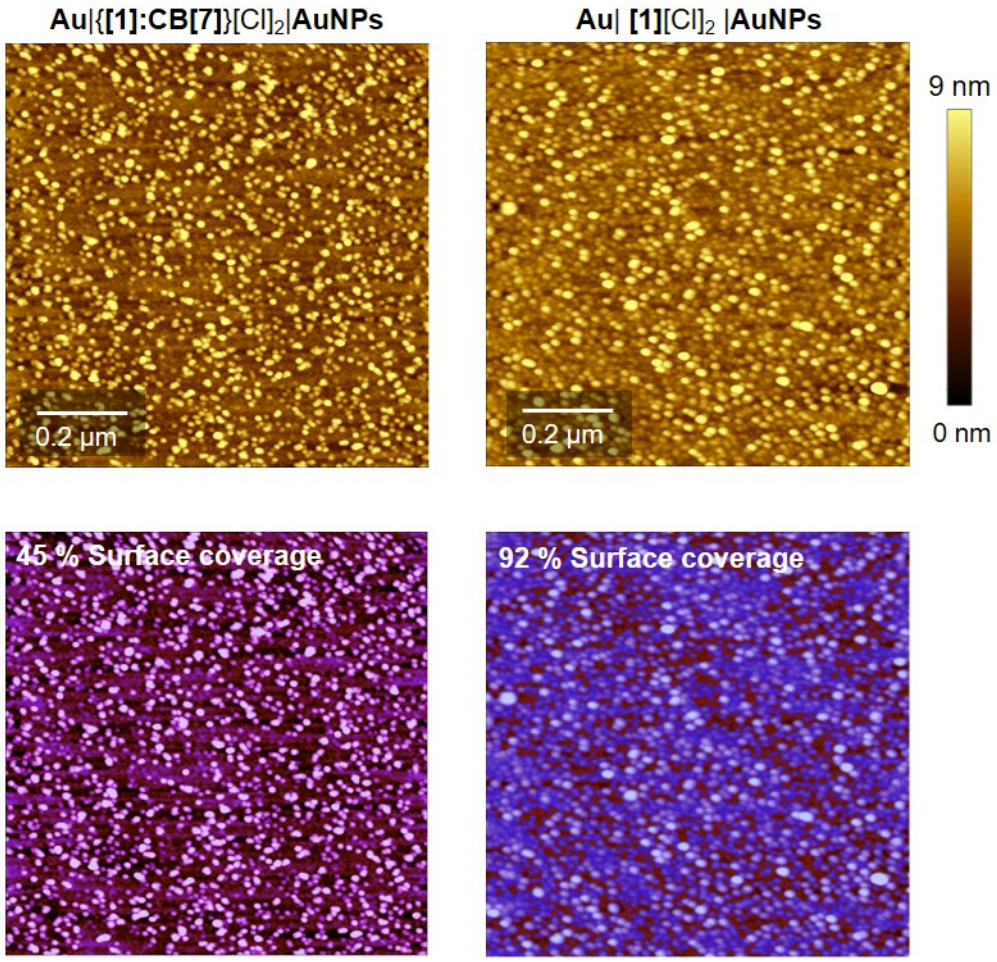

Figure S8. (top) AFM images of a SAM of {**[1]:CB[7]**}[Cl]$_2$ (left) and **[1]**[Cl]$_2$ (right) after incubation in a dispersion of AuNPs. (bottom) Same AFM images with the color mask unveiling AuNPs-free areas.

S6. I-V curves

For the **Au**|{**[1]:CB[7]**}$[Cl]_2$|**AuNP** structure when AuNPs less than 3 nm in diameter are used

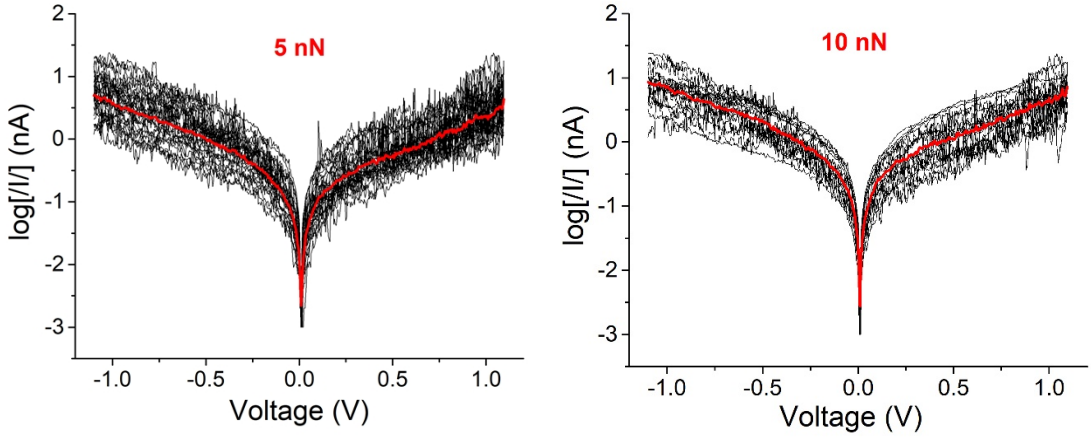

Figure S9. Log[|*I*|] versus voltage (ca. 250 curves) measured at a set point force of 5 and 10 nN. Averaged curves as shown as the red line.

For the **Au**|**1**$[Cl]_2$|**AuNP** structure

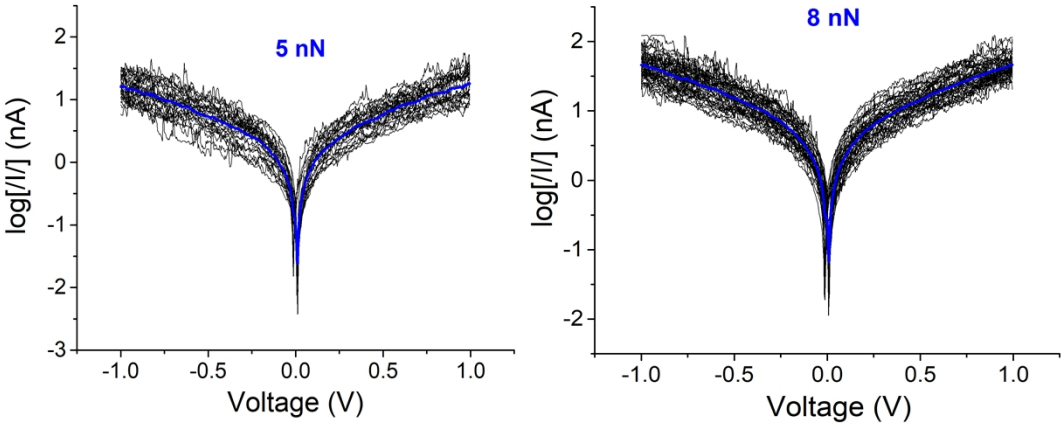

Figure S10. Log[|*I*|] versus voltage (ca. 120 curves) measured at a set point force of 5 and 8 nN. Averaged curves as shown as the blue line.

For the **Au**|**1**$[Cl]_2$|**AuNP** structure

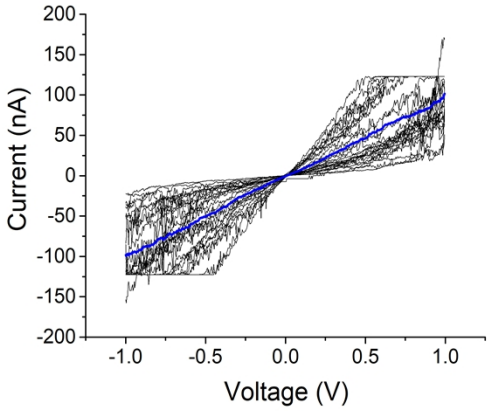

Figure S11. *I-V* curves (ca. 75 curves) measured at a set point force of 12 nN. Averaged curve is shown as the blue line. As the conductance increases substantially at this set point force, the current saturates at +/- 120 nA, limited by the current amplifier employed.

S7. Conductance *vs*. set-point force

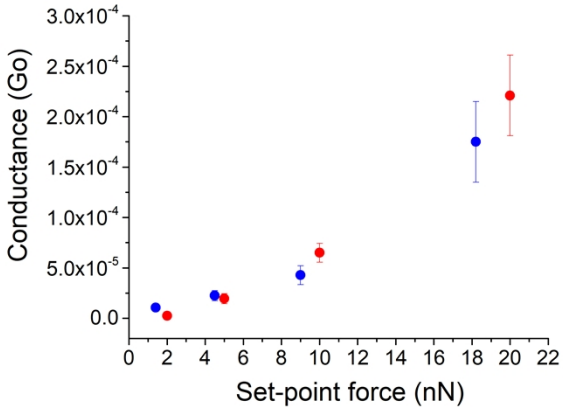

Figure S12. Conductance values versus the applied set-point force determined by locating the tip of the c-AFM onto an isolated gold nanoparticle less than 3 nm in diameter (red symbols) or directly above the film, free AuNPs areas in Figure 2b (blue symbols), for an **Au**|{**[1]:CB[7]**}$[Cl]_2$|**AuNP** structure.

S8. References

1. Fathalla, M.; Strutt, N. L.; Barnes, J. C.; Stern, C. L.; Ke, C. F.; Stoddart, J. F., Fluorescence Enhancement of a Porphyrin-Viologen Dyad by Pseudorotaxane Formation with Cucurbit[] Uril. *Eur. J. Org. Chem.* **2014**, *2014*, 2873-2877.
2. Freitag, M.; Gundlach, L.; Piotrowiak, P.; Galoppini, E., Fluorescence Enhancement of Di-P-Tolyl Viologen by Complexation in Cucurbit[7]Uril. *J. Am. Chem. Soc.* **2012**, *134*, 3358-3366.

3. Claveria-Gimeno, R.; Velazquez-Campoy, A.; Pey, A. L., Thermodynamics of Cooperative Binding of Fad to Human Nqo1: Implications to Understanding Cofactor-Dependent Function and Stability of the Flavoproteome. *Arch. Biochem. Biophys.* **2017**, *636*, 17-27.
4. Sauerbrey, G., Verwendung Von Schwingquarzen Zur Wagung Dunner Schichten Und Zur Mikrowagung. *Z. Phys.* **1959**, *155*, 206-222.
5. Bain, C. D.; Whitesides, G. M., Attenuation Lengths of Photoelectrons in Hydrocarbon Films. *J. Phys. Chem.* **1989**, *93*, 1670-1673.
6. Canet-Ferrer, J.; Coronado, E.; Forment-Aliaga, A.; Pinilla-Cienfuegos, E., Correction of the Tip Convolution Effects in the Imaging of Nanostructures Studied through Scanning Force Microscopy. *Nanotechnology* **2014**, *25*, 395703.